

# Radio Interferometric Observations of the Sun Using Commercial Dish TV Antennas

G. V. S. Gireesh<sup>1</sup> · C. Kathiravan<sup>1</sup> · Indrajit V. Barve<sup>1</sup> · R. Ramesh<sup>1</sup> 

© Springer ●●●

**Abstract** The radio astronomy group in the Indian Institute of Astrophysics (IIA) has been carrying out routine observations of radio emission from the solar corona at low frequencies ( $\approx 40\text{--}440\text{MHz}$ ) at the Gauribidanur observatory, about 100km north of Bangalore. Since IIA has been performing regular observations of the solar photosphere and chromosphere using different optical telescopes in its Kodaikanal Solar Observatory (KSO) also\*, the possibilities of obtaining two-dimensional radio images of the solar chromosphere using low-cost instrumentation to supplement the optical observations are being explored. As a part of the exercise, recently the group had developed prototype instrumentation for interferometric observations of radio emission from the solar chromosphere at high frequencies ( $\approx 11.2\text{GHz}$ ) using two commercial dish TV antennas. The hardware set-up and initial observations are presented.

**Keywords:** Sun, radio emission. Sun, eclipse. Radio telescopes, interferometry.

## 1. Introduction

Commercial dish TV antennas are parabolic structures designed to receive radio waves from a communication satellite. The antennas and the associated front end receiver systems have improved with advances in the TV systems. They

---

G. V. S. Gireesh  
[gireesh@iiap.res.in](mailto:gireesh@iiap.res.in)

C. Kathiravan  
[kathir@iiap.res.in](mailto:kathir@iiap.res.in)

Indrajit V. Barve  
[indrajit@iiap.res.in](mailto:indrajit@iiap.res.in)

R. Ramesh  
[ramesh@iiap.res.in](mailto:ramesh@iiap.res.in)

<sup>1</sup> Indian Institute of Astrophysics, 2nd Block, Koramangala, Bangalore 560034

\*see <https://www.iiap.res.in/kodai.htm>

operate typically over the frequency range 10.7-11.7GHz (Ku-band) and provide very good signal-to-noise ratio (SNR). It is well known that the Sun emits intense radio emission in the above frequency range with brightness temperature  $T_b \sim 10^4$ K. The emission is primarily due to thermal free-free mechanism, and originates in the upper chromosphere. The observed  $T_b = T_e(1 - e^{-\tau})$ , where  $T_e$  is the electron temperature and  $\tau$  is the optical depth of the medium. Therefore, estimates of  $T_b$  allows direct measurement of  $T_e$ , a ‘true’ temperature since it is independent of abundances or atomic physics. The optical depth ( $\tau$ ) factor in the above equation can be addressed using simultaneous observations at more than one frequency (see for e.g. Zirin, Baumert, and Hurford, 1991). It is well established that  $T_b$  is one of the basic properties of the Sun. Hence its routine monitoring is widely used as a diagnostic tool to understand the different types of temporal changes in the solar emission (Leblanc and Le Squeren, 1969; Tanaka *et al.*, 1973; Lantos and Avignon, 1975; Krüger *et al.*, 1986; Ramesh and Shanmugha Sundaram, 2000; Ramesh and Ebenezer, 2001; Ramesh *et al.*, 2006b; Kathiravan, Ramesh, and Subramanian, 2002; Kathiravan, Ramesh, and Nataraj, 2007; Selhorst *et al.*, 2011; Ramesh *et al.*, 2012b; Saint-Hilaire, Vilmer, and Kerdraon, 2013; Shibasaki, 2013; Tapping, 2013; Sasikumar Raja *et al.*, 2014; Mercier and Chambe, 2015; Ramesh *et al.*, 2020; Kumari, Morosan, and Kilpua, 2021). Motivated by the low-cost e-CALLISTO spectrometers which are successfully used for solar observations in the frequency range  $\sim 45-870$ MHz (Benz *et al.*, 2009) and considering off the shelf availability of dish TV antennas as well its associated receiver components at relatively low prices, we attempted observations of the Sun in the microwave frequency range mentioned above with a pair of commercial dish TV antennas. The observations were made in the correlation interferometer mode since it provides better sensitivity. Further, any contribution from the galactic background will also be negligible (Kraus, 1986). A two-element radio interferometer is also the building block of a synthesis imaging array (Thompson, Moran, and Swenson Jr., 2004). Some of the correlation radio interferometer arrays that routinely observe the Sun in the microwave frequency range with customized antennas are Nobeyama RadioHeliograph (NoRH; Nakajima *et al.*, 1994), Siberian Solar Radio Telescope (SSRT; Grechnev *et al.*, 2003), Expanded Owens Valley Solar Array (EOVSA; Nita *et al.*, 2016), and MingantU SpEctral Radioheliograph (MUSER; Yan *et al.*, 2021).

## 2. Antenna and Receiver System

Figure 1 shows the two commercial dish TV antennas set-up in the Gauribidanur observatory<sup>1</sup> for solar observations (Sastry, 1995; Ramesh, 2011). Each dish is parabolic reflector of diameter  $D \approx 62$ cm. Its an equatorial mount system. There is a feed horn and Low Noise Block (LNB, otherwise called the front end receiver) at the focus of the reflector. They receive and amplify the signal reflected by the parabolic dish. The LNB<sup>2</sup> has a noise figure (NF)  $\approx 0.6$ dB (corresponding noise

<sup>1</sup> see <https://www.iiap.res.in/?q=centers/radio>

<sup>2</sup> see <https://www.solid.sale/lmbf/ku-band-lnb/fs-108-ku-band-lnb>

temperature is  $\approx 45\text{K}$ ), and gain ( $G$ )  $\approx 60\text{dB}$ . The characteristic impedance ( $Z_0$ ) of the LNB is  $\approx 75\Omega$ . But the co-axial cables and other components used in the subsequent stages of the analog receiver system have  $Z_0 \approx 50\Omega$ . Due to this, there will be reflection of signal from the load and hence standing waves in the corresponding signal path. But we found that the reflected power due to the above impedance mismatch is small ( $\approx 4\%$ ). The measured reflection coefficient ( $\Gamma$ ) is  $\approx 0.2$ . This indicates that the amount of transmitted power that gets attenuated due to signal reflection is,  $10\log(1-\Gamma^2) \approx 0.2\text{dB}$ . Nevertheless we have connected a 1dB fixed attenuator between the LNB and the following amplifier (see Figure 2) to minimize the effects of the reflected signal<sup>3</sup>. The response pattern ('beam') of each dish has a theoretical half-power beamwidth (HPBW  $\approx 70^\circ \lambda/D$ ) of  $\approx 3.02^\circ \times 3.02^\circ$  (R.A.  $\times$  Dec.) at a typical frequency like 11.2GHz. Note that the above formula assumes that the electric field distribution is uniform across the aperture (see for e.g. Kraus, 1986). The feed horn receives radio frequency (RF) signal in the frequency range  $\approx 10.7\text{--}11.7\text{GHz}$ . The LNB has a frequency translating unit or a 'mixer' which converts the aforementioned RF signal to an intermediate frequency (IF) range of  $\approx 950\text{--}1950\text{MHz}$  by using a local oscillator (LO) signal of frequency 9.75GHz.

We had set-up a correlation interferometer with a separation of  $\approx 2.5\text{m}$  between the two dish antennas. The baseline between the antennas is oriented in the East-West direction. So, the theoretical angular resolution in that direction (for observations near the zenith), specified by separation between the interference fringes, is  $\approx 37'$  at 11.2GHz. The angular size of the Sun at 11GHz is  $\approx 33'$  (Fürst, Hirth, and Lantos, 1979). Since this is smaller than the aforementioned fringe spacing, Sun can be assumed to be a 'point' source for our observations. The corresponding resolution in the North-South direction is  $\approx 3.02^\circ$ , i.e. the HPBW of the dish mentioned above. A pair of motors, one for R.A. and other for Dec., are used for each dish antenna to tilt it towards the source position in the sky. Both the motors are controlled by a common Arduino board interfaced to a computer<sup>4</sup>. In the interferometric mode of observations the phase of LO signal at both the feeds must be synchronized. To achieve temporal coherence, we used a common external 25MHz clock signal to trigger the oscillators in the two LNBs. DC power supply for each LNB was provided using a Bias-Tee. It is a 3-port network<sup>5</sup> having (i) RF port where only RF signal can be extracted by blocking DC with the help of a capacitor, (ii) RF+DC port where DC is sent to bias the module (LNB in our case) and receive RF signal from the latter, and (iii) DC port where the DC source for biasing the module is connected. We used 'Nikou' make (10MHz-6GHz) Broadband Radio Frequency Microwave Coaxial Bias-Tee 1-50V, 0.5A (max) for the present work. The IF signal from each of the two antennas are independently amplified, filtered ( $\approx 1080\text{--}1450\text{MHz}$ ) and then transmitted to an analog receiver after downconverting to  $\approx 191.4\text{MHz}$  by mixing with another LO signal (triggered by the same 25MHz clock signal mentioned above) of frequency

---

<sup>3</sup> see <https://www.minicircuits.com/app/AN70-001.pdf>, etc.

<sup>4</sup> see <http://www.e-callisto.org/Hardware/Callisto-Hardware.html>

<sup>5</sup> see <https://www.microwaves101.com/encyclopedias/bias-tee>



**Figure 1.** The commercial dish TV antennas used in the Gauribidanur observatory for solar observations in the correlation interferometer mode.

1097.8MHz. A bandpass filter with center frequency 191.4MHz and bandwidth  $\approx 6$ MHz is used at the output of the ‘mixer’. In the analog receiver, the 191.4MHz signal is further amplified and downconverted to 10.7MHz by mixing with a LO signal (triggered by the same 25MHz clock signal mentioned above) of frequency 180.7MHz. Here a bandpass filter with center frequency 10.7 MHz and bandwidth  $\approx 1$ MHz is used at the output of the ‘mixer’. Some of the aforementioned LO and IF frequencies were chosen for the analog receiver system since the related RF components are available with us from our ongoing public outreach program<sup>6</sup>.

The 10.7MHz IF signal is split into in-phase and quadrature phase components using a quadrature power splitter and then connected to a 1-bit correlator which can be assembled with simple digital logic circuits (refer Figure 2). The 10.7MHz signal from the analog receiver are digitized using a 2-level (+1 or 0) high-speed comparator (AD790). The digitized signals are then sampled in a D-type flip-flop (74LS74) at a rate of 4MHz. Later they are passed on to an Ex-NOR gate for correlation. The output of the correlator are counted with the help of a 24-bit counter, which acts as an integrator (Ramesh, Sundara Rajan, and Sastry, 2006a). The counter output (i.e. the correlation count) are read by a computer via a 8-bit micro-controller (Microchip’s PIC16f877A). The integration time is  $\approx 1$ sec. Note that due to its simple design, the sensitivity of a 1-bit digital correlator is limited. It is  $\approx 0.64 \times$  the sensitivity of a corresponding

<sup>6</sup> see <https://www.iiap.res.in/centers/radio#pop>

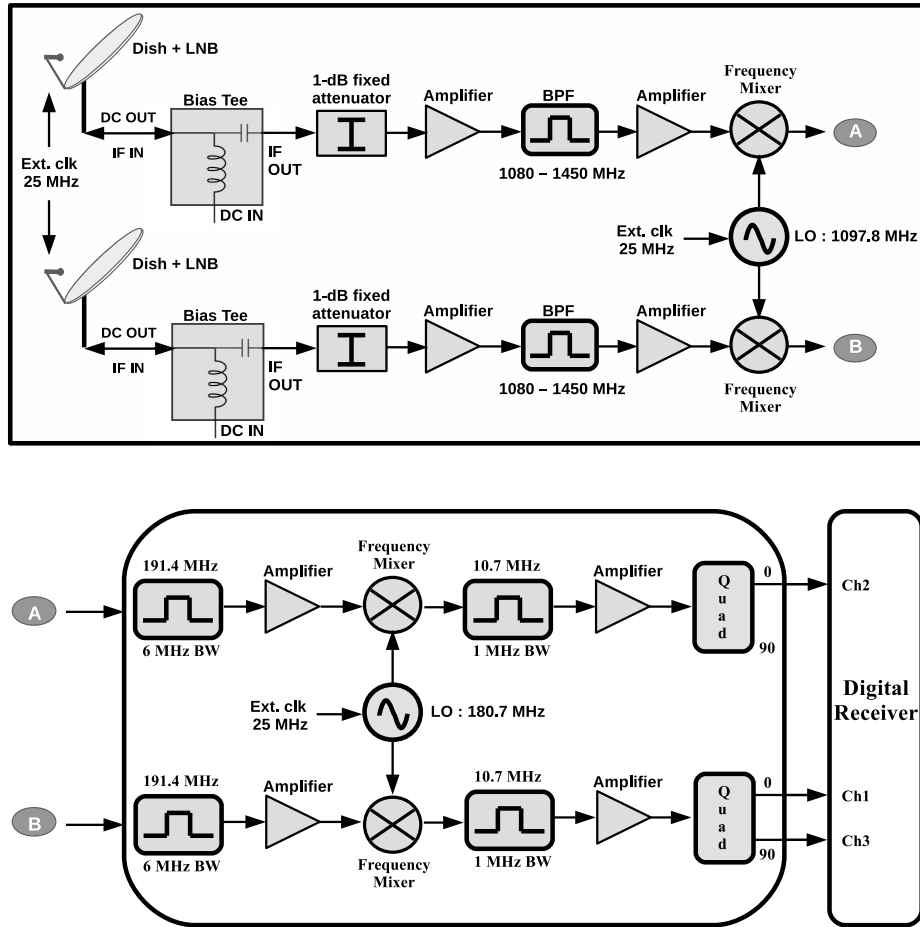


**Figure 2.** The analog receiver section corresponding to the two-element interferometer in Figure 1. ‘Quad’ is quadrature power-splitter. The 25MHz external clock is a common clock.

unquantized analog correlator (see for e.g. Thompson, Moran, and Swenson Jr., 2004). While this may not affect solar observations since the Sun is a ‘strong’ source, observations of ‘faint’ calibrator sources could be restricted. For e.g., the  $T_b$  of a calibrator source like the Moon is  $\approx \frac{1}{40} \times T_b$  of the Sun in the above frequency range (see Section 3).

### 3. Observations

Figures 3 and 4 show observations of the Moon (9 June 2020) and the Sun (20 June 2020) with the above described set-up (i.e. the Ku-band interferometer). Note that the average angular size of the Moon is  $\approx 31'$  (see for e.g. Kraus, 1986). So it can be also considered as a ‘point’ source for our observations, similar to the Sun (see Section 2). The observations were carried out in the drift scan

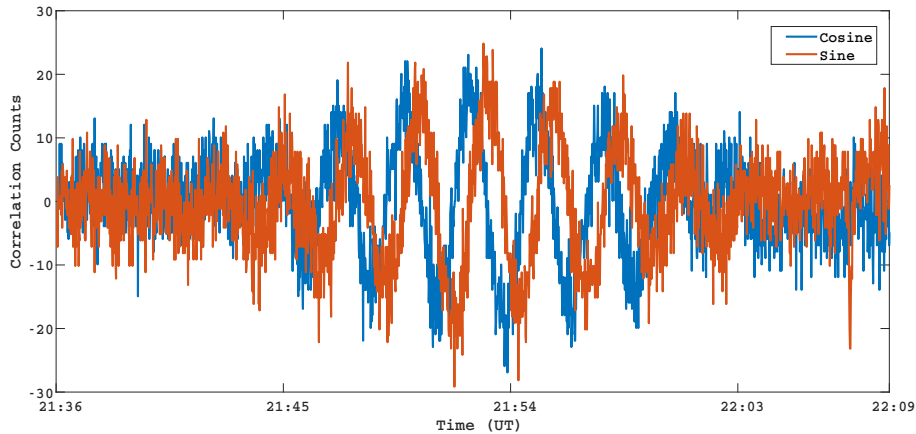


**Figure 3.** Observations of the Moon on 9 June 2020 at  $\approx 11.2$ GHz during its transit over the local meridian in Gauribidanur.

mode after tilting the two dish antennas towards the direction of the sources using the motors as mentioned earlier. While the ‘cosine’ fringes correspond to the correlation between in-phase 10.7MHz IF signal from the two antennas, the ‘sine’ fringes correspond to the correlation between in-phase 10.7MHz IF signal from one of the antennas and quadrature phase 10.7MHz IF signal from the other antenna. The observed fringe spacing in Figure 4 is  $\approx 40'$ . The half-width of the fringe envelope is  $\approx 3.2^\circ$ . The observations were carried out when hour angle of the Sun was  $\approx 9^\circ$  to the east of the local meridian in Gauribidanur. The declination of the Sun was  $\approx 23^\circ 30'N$ . Taking into consideration the projected baseline length ( $\approx 2.3$ m) as seen by the source, the aforementioned fringe spacing derived from the observations is reasonably consistent with the expected value mentioned earlier. The extent of the observed fringe envelope is supposed to be same as the theoretical HPBW ( $\approx 3.02^\circ$ ) of the individual dish antenna. But it is  $\approx 1.06\times$  wider. In fact estimates from observations on different days also gave the same result (i.e.  $\approx 3.2^\circ$ ). Therefore it is likely that the above difference is most likely due to the design parameters of the dish. For e.g. if the electric field distribution across the aperture is parabolic, then  $HPBW \approx 73^\circ \lambda/D$  (see for e.g. Kraus, 1986).

Maximum radiation from the Moon is usually received at Earth  $\approx 3-4$  days after a Full Moon day<sup>7</sup>. In the present case, 5 June 2020 was a Full Moon day. Based on this, we calculated the theoretical  $T_b$  of the Moon corresponding to the observations in Figure 3 on 9 June 2020 to be  $\approx 227$ K (Linsky, 1973). Using this, we then estimated the  $T_b$  of the Sun in Figure 4 as  $T_{bSun} = (x/y)T_{bMoon}$ , where  $x$  and  $y$  are the peak visibility amplitudes of the Sun and Moon, respectively. The visibility amplitudes were calculated as  $\sqrt{C_t^2 + S_t^2}$ , where  $C_t$  and  $S_t$  are the amplitudes of the cosine and sine fringes at time  $t$ . The resultant  $T_b$  of the Sun was found to be  $\approx 9266$ K. This is consistent with microwave brightness temperature spectrum of the ‘quiet’ Sun (Zirin, Baumert, and Hurford, 1991). The

<sup>7</sup> see <https://doi.org/10.3929/ethz-a-004322130>

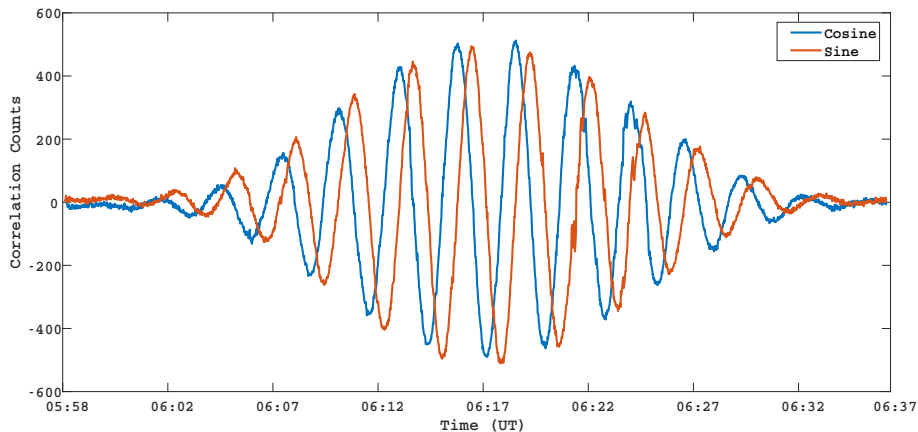


**Figure 4.** Same as Figure 3, but observations of the Sun on 20 June 2020.

possible causes of error in the  $T_b$  of the Sun mentioned above are uncertainties in the  $T_b$  of the Moon (Iwai *et al.*, 2017), rainfall, and variation in sky-noise temperature ( $T_{sky}$ ) as a function of elevation angle of the radio source. But there were no rain during the present observations. Further, both the Sun and Moon were observed nearly at the same elevation ( $\approx 4^\circ$  and  $\approx -5^\circ$ , respectively). However, observations of the Sun and Moon were at different epochs and the receivers were not temperature controlled also. So there could be gain variations. We verified and corrected this by monitoring the Ku-band transmission from geostationary satellites INSAT 3A & 4A (located at  $\approx 93.5^\circ\text{E}$  longitude and  $\approx 83^\circ\text{E}$  longitude, respectively)<sup>8</sup>. The equivalent isotropically radiated power (EIRP) of the above two satellites in the frequency range 11-11.25GHz and 11.55-11.70GHz are  $\approx 48\text{dBW}$  and  $\approx 52\text{dBW}$ , respectively. Note that the coordinates of Gauribidanur observatory are  $\approx 77^\circ 26'\text{E}$  longitude and  $\approx 13^\circ 36'\text{N}$  latitude. We observe the aforementioned satellite signal transmission everyday, particularly before and after the observations of the Sun and Moon. The maximum variation in a day is  $\approx 2.8\%$ . Having identified the different possible sources of error, we calculated the overall error in the  $T_b$  of the Sun as follows: by using 2nd order Gaussian fit to the observations of the Moon in Figure 3 we estimated the SNR to be  $\approx 4.4$ . Since  $T_b$  of the Moon is  $\approx 227\text{K}$ , the above SNR gives a temperature of  $\approx 52\text{K}$  for the noise fluctuations in the observations. This is the system temperature ( $T_{sys}$ ). It depends primarily on the sky noise temperature ( $T_{sky}$ ) and noise temperature of the LNB (i.e.  $T_{rcvr}$ ). Assuming  $T_{sky}$  at 11.2GHz for observations near the zenith to be  $\approx 10\text{K}$  (see for e.g. Kraus, 1986), we find  $T_{rcvr} \approx 42\text{K}$ . This is reasonably consistent with the noise temperature of the LNB mentioned in Section 2. Therefore in the present case,  $T_b$  of the Moon is  $\approx 227 \pm 52\text{K}$ , and  $T_b$  of the Sun is  $\approx 9266 \pm 2108\text{K}$ .

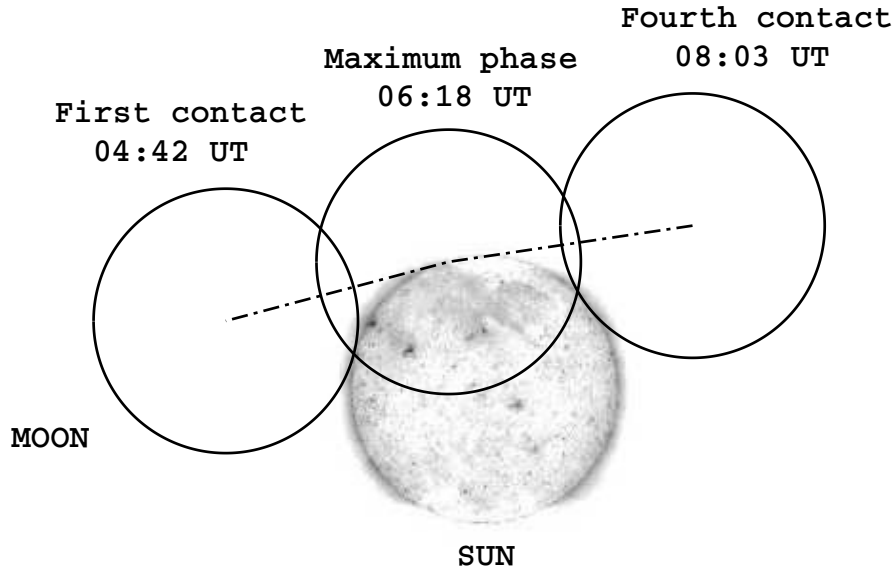


**Figure 5.** Positions of the Moon during the first contact, maximum phase, and fourth contact of the 21 June 2020 solar eclipse (as seen from Gauribidanur observatory) overlaid on the 211Å image of the Sun obtained the same day at  $\approx 06:30$  UT with the Atmospheric Imaging Assembly (AIA; Lemen *et al.*, 2012) on board the Solar Dynamics Observatory (SDO). North is straight up and east is to the left.

### 3.1. The Solar Eclipse of 21 June 2020

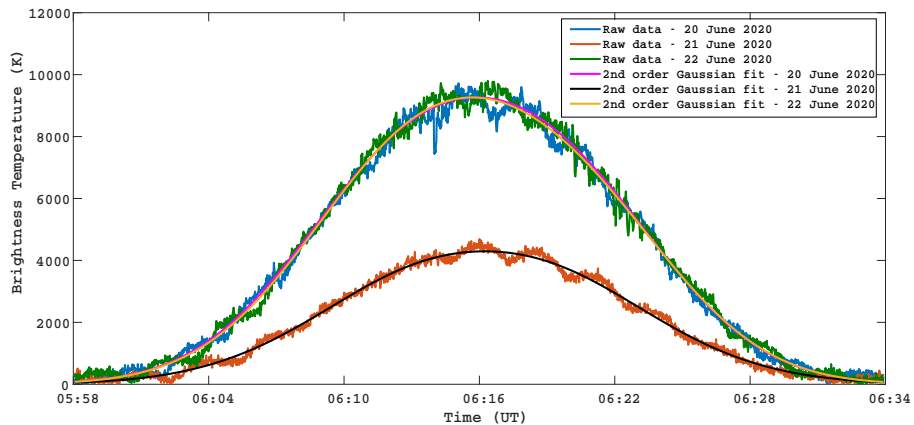
The solar eclipse of 21 June 2020 was partial at Gauribidanur observatory with magnitude  $\approx 0.493$  and obscuration  $\approx 38.33\%$ <sup>9</sup>. Note that the solar eclipses are always partial at radio frequencies since the angular sizes of the ‘radio’ Sun in the frequency range over which it is typically observed from the ground are larger compared to that of the Moon. While the average angular size of the Moon is  $\approx 31'$  (see Section 3), the corresponding values for the ‘radio’ Sun at 11 GHz and 80 MHz (the frequencies mentioned in this paper) are  $\approx 33'$  and  $\approx 38'$ , respectively (Borovik, 1980; Ramesh *et al.*, 2006b). The first contact of Moon with the limb of the Sun (i.e. the solar photosphere) occurred at  $\approx 04:42$  UT. The maximum phase of the eclipse was at  $\approx 06:18$  UT. The fourth contact was at  $\approx 08:03$  UT (Figure 5). Based on our experience with radio observations at low frequencies during solar eclipses in the past (Ramesh, Subramanian, and Sastry, 1999; Ramesh *et al.*, 2012a; Kathiravan *et al.*, 2011), we carried out observations of the Sun with the Ku-band interferometer at  $\approx 11.2$  GHz for a few days around 21 June 2020 in the drift scan mode as mentioned earlier.

Figure 6 shows the results of our observations on 20 June 2020 (the day before the eclipse), 21 June 2020 (during the eclipse), and 22 June 2020 (day

<sup>8</sup> see [https://en.wikipedia.org/wiki/Indian\\_National\\_Satellite\\_System](https://en.wikipedia.org/wiki/Indian_National_Satellite_System)

<sup>9</sup> see <https://www.timeanddate.com/eclipse/map/2020-june-21>





**Figure 6.** Observations of the Sun with Ku-band interferometer on 20, 21, & 22 June 2020 in the transit mode after tilting the antennas towards the direction of the Sun.

after the eclipse). The observations on 21 June 2020 were during the maximum phase of the eclipse. The profiles shown correspond to the visibility amplitudes calculated from the observed cosine and sine fringes as described in Section 3. The estimated  $T_b$  of the Sun at  $\approx 11.2$ GHz (after calibration using observations of the Moon with the same set-up) on the above three days are  $\approx 9266$ K,  $4294$ K, and  $9263$ K, respectively. The  $T_b$  on 21 June 2020 is lesser by  $\approx 54\%$ . A closer look of Figure 5 indicates that three noticeable active regions in the northern hemisphere of the Sun were fully occulted during the maximum phase of the eclipse. This could be the reason for the aforementioned reduction in  $T_b$  (though the eclipse obscuration was only 38%) since radio emission associated with the active regions constitute a significant fraction of the total emission from the Sun (see for e.g. Covington, 1947; Mayfield, Chapman, and Straka, 1971; Kathiravan *et al.*, 2011). An inspection of data obtained with the Gauribidanur RAdiohe-liograPH (GRAPH; Ramesh *et al.*, 1998, Ramesh *et al.*, 2014) at 53MHz and 80MHz during the eclipse on 21 June 2020 also reveal a similar reduction in the estimated  $T_b$  as compared to the corresponding values observed on the day before as well as after the eclipse.

#### 4. Summary

We have reported successful radio interferometric observations of the Sun at  $\approx 11.2$ GHz using two commercial dish TV antennas operating in the Ku-band ( $\approx 10.7$ - $11.7$ GHz). The results obtained are encouraging for our plans to set up an array of such antennas for dedicated and synoptic two-dimensional spectroscopic imaging observations of the Sun in the above frequency range with minimal budget. Work is in progress to fine tune the pointing accuracy of the dishes and develop a FPGA based spectrocorrelator to observe over the entire 10.7-11.7 GHz frequency band.

**Acknowledgments** We express our gratitude to the staff of the Gauribidanur observatory for their help in setting up the antenna/receiver systems, and carrying out the observations. The SDO/AIA data are courtesy of the NASA/SDO and the AIA science teams. We thank the referee for his/her kind comments which helped us to improve the manuscript.

**Declaration:** The authors declare that there are no conflicts of interest.

## References

- Benz, A.O., Monstein, C., Meyer, H., Manoharan, P.K., Ramesh, R., Altyntsev, A., Lara, A., Paez, J., Cho, K.-S.: 2009, A World-Wide Net of Solar Radio Spectrometers: e-CALLISTO. *Earth, Moon & Planets* **104**, 277. DOI. ADS. [Benz09]
- Borovik, V.N.: 1980, RATAN-600 Measurements of the 2cm-4cm Radio Brightness Distribution Over the Disk of the Quiet Sun. *Sov. Astron. Lett.* **6**, 236. DOI. ADS. [Borovik80]
- Covington, A.E.: 1947, MicroWave Solar Noise Observations During the Partial Eclipse of November 23, 1946. *Nature* **159**, 405. DOI. ADS. [Covington47]
- Fürst, E., Hirth, W., Lantos, P.: 1979, The radius of the Sun at centimeter waves and the brightness distribution across the disk. *Solar Phys.* **63**, 253. DOI. ADS. [Furst79]
- Grechnev, V.V., Lesovoi, S.V., Smolkov, G.Y., Krissinel, G.B., Zandanov, V.G., et al.: 2003, The Siberian Solar Radio Telescope: the current state of the instrument, observations, and data. *Solar Phys.* **216**, 239. DOI. ADS. [Grechnev03]
- Iwai, K., Shimojo, M., Asayama, S., Minamidani, T., White, S.M., Bastian, T.S., Saito, M.: 2017, The Brightness Temperature of the Quiet Solar Chromosphere at 2.6 mm. *Solar Phys.* **292**, 22. DOI. ADS. [Iwai17]
- Kathiravan, C., Ramesh, R., Nataraj, H.S.: 2007, The Post-Coronal Mass Ejection Solar Atmosphere and Radio Noise Storm Activity. *Astrophys. J. Lett.* **656**, L37. DOI. ADS. [Kathiravan07]
- Kathiravan, C., Ramesh, R., Subramanian, K.R.: 2002, Metric Radio Observations and Ray-tracing Analysis of the Onset Phase of a Solar Eruptive Event. *Astrophys. J. Lett.* **567**, L93. DOI. ADS. [Kathiravan02]
- Kathiravan, C., Ramesh, R., Indrajit V. Barve, Rajalingam, M.: 2011, Radio Observations of the Solar Corona During an Eclipse. *Astrophys. J.* **730**, 91. DOI. ADS. [Kathiravan11]
- Kraus, J.D.: 1986, *Radio Astronomy 2nd Ed.*, Cygnus-Quasar, Ohio. [Kraus86]
- Krüger, A., Hildebrandt, J., Bogod, V.M., Korzhavin, A.M., Ahmedov, S.B., Gelfreikh, G.B.: 1986, A Study of RATAN-600 Observations of Solar S-Component Sources. *Solar Phys.* **105**, 111. DOI. ADS. [Kruger86]
- Kumari, A., Morosan, D.E., Kilpua, E.K.J.: 2021, On the Occurrence of Type IV Solar Radio Bursts in Solar Cycle 24 and Their Association with Coronal Mass Ejections. *Astrophys. J.* **906**, 79. DOI. ADS. [Anshu21]
- Lantos, P., Avignon, Y.: 1975, The metric quiet Sun during two cycles of activity and the nature of the coronal holes. *Astron. Astrophys.* **41**, 137. ADS. [Lantos75]
- Leblanc, Y., Le Squeren, A.M.: 1969, Dimensions, Temperature and Electron Density of the Quiet Corona. *Astron. Astrophys.* **1**, 239. ADS. [Leblanc69]
- Lemen, J.R., Title, A.M., Akin, D.J., Boerner, P.F., Chou, C., et al.: 2012, The Atmospheric Imaging Assembly (AIA) on the Solar Dynamics Observatory (SDO). *Solar Phys.* **272**, 17. DOI. ADS. [Lemen12]
- Linsky, J.L.: 1973, A Recalibration of the Quiet Sun Millimeter Spectrum Based on the Moon as an Absolute Radiometric Standard. *Solar Phys.* **28**, 409. DOI. ADS. [Linsky73]
- Mayfield, E.B., Chapman, G.A., Straka, R.M.: 1971, Eclipse of Radio Emission on 7 March, 1970 at 10 cm Wavelength from the Active Region Associated with McMath Plage 10618. *Solar Phys.* **21**, 460. DOI. ADS. [Mayfield71]
- Mercier, C., Chambe, G.: 2015, Electron density and temperature in the solar corona from multifrequency radio imaging. *Astron. Astrophys.* **583**, A101. DOI. ADS. [Mercier15]
- Nakajima, H., Nishio, M., Enome, S., Shibasaki, K., Takano, T., et al.: 1994, The Nobeyama radioheliograph. *Proc. IEEE* **82**, 705. ADS. [Nakajima94]
- Nita, G.M., Hickish, J., MacMahon, D., Gary, D.E.: 2016, EOVS Implementation of a Spectral Kurtosis Correlator for Transient Detection and Classification. *J. Astron. Instr.* **5**, 1641009. DOI. ADS. [Nita16]

- Ramesh, R.: 2011, Low frequency solar radio astronomy at the Indian Institute of Astrophysics (IIA). In: Choudhuri, A.R., Banerjee, D. (eds.) *First Asia-Pacific Solar Physics Meeting*, Astron. Soc. India: Conf. Ser. **2**, ???, 55. [ADS](#). [Ramesh11]
- Ramesh, R., Ebenezer, E.: 2001, Decameter Wavelength Observations of an Absorption Burst from the Sun and Its Association with an X2.0/3B Flare and the Onset of a 'Halo' Coronal Mass Ejection. *Astrophys. J. Lett.* **558**, L141. [DOI](#). [ADS](#). [Ramesh01]
- Ramesh, R., Shanmugha Sundaram, G.A.: 2000, Type I radio bursts and the minimum between sunspot cycles 22 & 23. *Astron. Astrophys.* **364**, 873. [ADS](#). [Ramesh00]
- Ramesh, R., Subramanian, K.R., Sastry, C.V.: 1999, Eclipse Observations of Compact Sources in the Outer Solar Corona. *Solar Phys.* **185**, 77. [DOI](#). [ADS](#). [Ramesh99]
- Ramesh, R., Sundara Rajan, M.S., Sastry, C.V.: 2006a, The 1024 channel digital correlator receiver of the Gauribidanur radioheliograph. *Exp. Astron.* **21**, 31. [DOI](#). [ADS](#). [Ramesh06a]
- Ramesh, R., Subramanian, K.R., Sundara Rajan, M.S., Sastry, C.V.: 1998, The Gauribidanur Radioheliograph. *Solar Phys.* **181**, 439. [DOI](#). [ADS](#). [Ramesh98]
- Ramesh, R., Nataraj, H.S., Kathiravan, C., Sastry, C.V.: 2006b, The Equatorial Background Solar Corona during Solar Minimum. *Astrophys. J.* **648**, 707. [DOI](#). [ADS](#). [Ramesh06b]
- Ramesh, R., Kathiravan, C., Indrajit V. Barve, Rajalingam, M.: 2012a, High Angular Resolution Radio Observations of a Coronal Mass Ejection Source Region at Low Frequencies during a Solar Eclipse. *Astrophys. J.* **744**, 165. [DOI](#). [ADS](#). [Ramesh12a]
- Ramesh, R., Kathiravan, C., Anna Lakshmi, M., Gopalswamy, N., Umopathy, S.: 2012b, The Location of Solar Metric Type II Radio Bursts with Respect to the Associated Coronal Mass Ejections. *Astrophys. J.* **752**, 107. [DOI](#). [ADS](#). [Ramesh12b]
- Ramesh, R., Kathiravan, C., Sundara Rajan, M.S., Indrajit V. Barve, Rajalingam, M.: 2014, Solar observations at low frequencies with the Gauribidanur radioheliograph. In: Chengalur, J.N., Gupta, Y. (eds.) *The Metrewavelength Sky*, Astron. Soc. India: Conf. Ser. **13**, ???, 19. [ADS](#). [Ramesh14]
- Ramesh, R., Kumari, A., Kathiravan, C., Ketaki, D., Rajesh, M., Vrunda, M.: 2020, Low-Frequency Radio Observations of the Quiet Corona During the Descending Phase of Sunspot Cycle 24. *Geophys. Res. Lett.* **47**, e90426. [DOI](#). [ADS](#). [Ramesh20]
- Saint-Hilaire, P., Vilmer, N., Kerdran, A.: 2013, A Decade of Solar Type III Radio Bursts Observed by the Nancy Radioheliograph 1998-2008. *Astrophys. J.* **762**, 60. [DOI](#). [ADS](#). [Saint13]
- Sasikumar Raja, K., Ramesh, R., Hariharan, K., Kathiravan, C., Wang, T.J.: 2014, An Estimate of the Magnetic Field Strength Associated with a Solar Coronal Mass Ejection from Low Frequency Radio Observations. *Astrophys. J.* **796**, 56. [DOI](#). [ADS](#). [Sasikumar14]
- Sastry, C.V.: 1995, The Decameter and Meter Wave Radiotelescopes in India and Mauritius. *Space Sci. Rev.* **72**, 629. [DOI](#). [ADS](#). [Sastry95]
- Selhorst, C.L., Giménez De Castro, C.G., Válio, A., Costa, J.E.R., Shibasaki, K.: 2011, The Behavior of the 17 GHz Solar Radius and Limb Brightening in the Spotless Minimum XXIII/XXIV. *Astrophys. J.* **734**, 64. [DOI](#). [ADS](#). [Selhorst11]
- Shibasaki, K.: 2013, Long-Term Global Solar Activity Observed by the Nobeyama Radioheliograph. *Publ. Astron. Soc. Japan* **65**, S17. [DOI](#). [ADS](#). [Shibasaki13]
- Tanaka, H., Castelli, J.P., Covington, A.E., Krüger, A., Landecker, T.L., Tlamicha, A.: 1973, Absolute Calibration of Solar Radio Flux Density in the Microwave Region. *Solar Phys.* **29**, 243. [DOI](#). [ADS](#). [Tanaka73]
- Tapping, K.F.: 2013, The 10.7 cm solar radio flux ( $F_{10.7}$ ). *Space Weather* **11**, 394. [DOI](#). [ADS](#). [Tapping13]
- Thompson, A.R., Moran, J.M., Swenson Jr., G.W.: 2004, *Interferometry and Synthesis in Radio Astronomy 2nd Ed.*, WILEY-VCH, Weinheim. [Thompson04]
- Yan, Y., Chen, Z., Wang, W., Liu, F., Geng, L., Chen, L., Tan, C., Chen, X., Su, C., Tan, B.: 2021, Mingantu Spectral Radioheliograph for Solar and Space Weather Studies. *Frontiers Astron. Space Sci.* **8**, 20. [DOI](#). [ADS](#). [Yan21]
- Zirin, H., Baumert, B.M., Hurford, G.: 1991, The Microwave Brightness Temperature Spectrum of the Quiet Sun. *Astrophys. J.* **370**, 779. [DOI](#). [ADS](#). [Zirin91]